كلية الهندسة بشبرا
FACULTY OF ENGINEERING AT SHOUBRA
ERJ
PRINT ISSN 3009-6049
ONLINE ISSN 3009-6022

ENGINEERING RESEARCH JOURNAL (ERJ)
Volume (54),Issue (2)
April 2025, pp:168-178
https://erjsh.journals.ekb.eg

High-Performance Direct Torque Control of Induction Motor Drives: A Comparative Study of Hysteresis and Space Vector Modulation Schemes

Shady Mamdouh Sadek [1,*], Al-Waseem Ahmed Shaheen[1], Maged Al-Barashi[2]

[1]*Electrical Power Engineering Department, International Academy for Engineering and Media Sciences (IAEMS), Cairo, Egypt*
[2] *School of Aeronautics and Astronautics, Guilin University of Aerospace Technology, Guilin, 541004, China*
**Corresponding author*

E-mail address: shady.mamdouh.sadek@iaems.edu.eg, elwaseem.ahmed@iaems.edu.eg, dr_albarashi@yahoo.com

Abstract: Direct Torque Control (DTC) is a prominent control strategy for induction motor drives, valued for its fast dynamic response and minimal dependence on motor parameters. This paper presents a comparative analysis of two DTC schemes: conventional hysteresis-based DTC and Space Vector Modulation (SVM)-based DTC, focusing on their performance in high-dynamic-response drive systems. The conventional hysteresis DTC, despite its simplicity and rapid torque response, suffers from high torque and flux ripples and variable switching frequency, which can degrade drive efficiency and precision. In contrast, SVM-DTC mitigates these drawbacks by maintaining a constant switching frequency, reducing torque ripple, and enhancing overall system efficiency, albeit at the cost of increased computational complexity. The study evaluates these schemes in terms of torque and flux control accuracy, switching losses, and dynamic response, providing a comprehensive assessment of their suitability for modern high-performance motor drive applications. MATLAB/Simulink is used to make modeling and simulation of the two schemes. From the obtained simulation results, both conventional and SVM-DTC have extremely fast torque dynamics. A key difference is the apparent smoothness of the torque, flux, and current waveforms of SVM-DTC compared to the conventional DTC. SVM-DTC provides a 30% reduction in torque ripples and a 20% increased improvement in overall system efficiency compared to conventional DTC. Additionally, SVM-DTC achieves a 2% faster dynamic response. However, SVM-DTC requires a more complex algorithm due to the SVM calculation itself, compared to the simpler hysteresis comparators and lookup table of conventional DTC.

Keywords: *Direct torque control, Induction motor drives, space vector modulation*

1. INTRODUCTION

Induction motors (IMs) form the backbone of industrial mechanization and increasingly power transportation systems, celebrated for their inherent robustness, relatively low maintenance requirements, and favorable economics. Despite these advantages, harnessing their full dynamic potential, particularly in applications demanding precise speed or torque control alongside high energy efficiency, mandates sophisticated control strategies. Direct Torque Control (DTC) is considered as a prominent technique for the control of induction motors (IMs), offering high dynamic responses for both torque and flux without the need for coordinate transformations or pulse-width modulation (PWM) strategies compared to the Field Oriented Control (FOC) technique which relies on machine parameters and requires axes transformation and pulse width modulation. Traditionally, DTC employs hysteresis controllers to maintain torque and flux within predefined hysteresis bands, directly selecting the suitable voltage vectors from a predefined look-up table to achieve the desired performance. However, this conventional approach often results in high torque and flux ripples and poor performance at low speeds due to the variable switching frequency inherent in hysteresis-based methods [1].

To address these challenges, the integration of Space Vector Modulation (SVM) into DTC schemes has been proposed. SVM-DTC aims to regulate the switching frequency, thereby reducing torque and flux ripples and enhancing the overall performance of induction motor drives [2]–[5]. Recent studies have demonstrated that SVM-based DTC can significantly improve the steady-state and dynamic behavior of IMs. For instance, research indicates that incorporating SVM into DTC strategies leads to a substantial reduction in torque ripples and

mitigates the random variation problem of switching frequency across a wide range of speed or torque controls [6]. Additionally, the use of advanced controllers, such as Integral-Proportional (IP) speed regulators, in conjunction with SVM-DTC has been shown to ensure good dynamic performance and minimize peak overshoot in speed responses [7].

Further advancements include the application of nonlinear control techniques like backstepping, combined with SVM-DTC, to enhance robustness against uncertainties and external disturbances, thereby reducing torque and flux ripples. Studies have proposed improved DTC strategies utilizing robust backstepping controllers along with stator resistance compensators to achieve better performance, especially at low speeds [8].

For instance, research demonstrates that reducing hysteresis bandwidth can mitigate ripples but increases switching frequency, leading to higher inverter losses [9]. Efforts to enhance this method include adaptive hysteresis band techniques [8] and integration with intelligent control strategies like fuzzy logic [10], which reduce ripples by up to 50% compared to classical DTC.

Moreover, the adoption of fractional-order sliding mode control (FOSMC) techniques within SVM-DTC frameworks has been explored to achieve quick response times and further reduce torque ripple. These approaches leverage the benefits of fractional calculus to enhance the robustness and performance of induction motor drives [11].

Comparative studies consistently highlight the trade-off between the simplicity and robustness of Hysteresis-DTC versus the superior steady-state performance (lower ripple, fixed switching frequency) of SV-DTC [12]–[14]. The choice between them often depends critically on the specific application requirements – Hysteresis-DTC might suffice for low-cost, less demanding applications, while SV-DTC is preferred for high-performance drives where smooth operation and efficiency are paramount [15].

Recent advancements often focus on enhancing SV-DTC's robustness or Hysteresis-DTC's ripple performance. Model Predictive Control (MPC) techniques applied to DTC, often resembling SV-DTC in structure but using optimization, have shown promise in achieving fast dynamics with constraint handling [16]–[18]. Hybrid approaches, which might switch between Hysteresis and SV-DTC logic based on operating conditions (e.g., transient vs. steady-state), continue to be explored to leverage the benefits of both [19]. Furthermore, the integration of machine learning and fuzzy logic techniques aims to improve adaptivity and performance tuning for both strategies [20]–[23].

This paper aims to provide a comprehensive comparison between conventional hysteresis-based DTC and SVM-based DTC for induction motors. By evaluating key performance metrics such as torque ripple, dynamic response, steady-state behavior, switching frequency effects, and computational complexity, this study seeks to interpret the advantages and limitations of each control strategy, thereby informing the selection of appropriate methods for specific applications.

The paper is structured as follows. Section one is an introduction and literature review about DTC applied to IMs drives. Section two gives the modeling of IMs in the stationary reference frame. Section three presents an overview about the principles of both conventional hysteresis DTC and SVM-DTC methods. Section four shows the simulation of DTC in IMs. Section five gives the results and discussions. And finally, section six outlines the references.

2. MODELING OF IM IN THE STATIONARY REFERENCE FRAME (ALPHA- BETA PLANE)

The dynamic equations for the three phase induction motor in the stationary reference frame are as follows:

The stator voltage space vector (u_s) of the machine in the stationary reference frame are given by:

$$u_{s\alpha} = R_s i_{s\alpha} + L_s\left(\frac{di_{s\alpha}}{dt}\right) + L_m\left(\frac{di_{r\alpha}}{dt}\right) \quad (1)$$

$$u_{s\beta} = R_s i_{s\beta} + L_s\left(\frac{di_{s\beta}}{dt}\right) + L_m\left(\frac{di_{r\beta}}{dt}\right) \quad (2)$$

The rotor voltage equations of the machine in the stationary reference frame are given by:

$$0 = L_m\left(\frac{di_{s\alpha}}{dt}\right) + R_r i_{r\alpha} + L_r\left(\frac{di_{r\alpha}}{dt}\right) \quad (3)$$

$$0 = L_m\left(\frac{di_{s\beta}}{dt}\right) + R_r i_{r\beta} + L_r\left(\frac{di_{r\beta}}{dt}\right) \quad (4)$$

The mechanical system equation is given by:

$$(J/p)\left(\frac{d\omega_r}{dt}\right) = \frac{3}{2}p\left[\left(\psi_{s\alpha}i_{s\beta} - \psi_{s\beta}i_{s\alpha}\right) - i_{r\alpha}\psi_{r\beta} + i_{r\beta}\psi_{r\alpha}\right] - T_L \quad (5)$$

3. PRINCIPLE OF CONVENTIONAL HYSTERESIS DTC

3.1. TORQUE CONTROL

Direct Torque Control (DTC) is considered as a prominent high-performance control strategy for induction motor drives, primarily due to its ability to

achieve rapid and decoupled control for both motor torque and stator flux magnitude without depending on traditional current controller loops or complex coordinate transformations that are required in field-oriented control (FOC). The main principle requires the direct application of discrete inverter voltage vectors selected from a predefined look up table called "Switching Table "based on the real-time errors between the reference and estimated values of torque and flux [24]. By employing hysteresis comparators, these errors are constrained within predefined bands, ensuring fast dynamic responses. The two dominant DTC structures are the conventional hysteresis-based DTC (C-DTC), known for its simplicity, and Space Vector Modulation DTC (SVM-DTC), which aims to address some inherent limitations of the classical approach [25].

The classical DTC methodology utilizes multi-level hysteresis controllers to directly handle torque and stator flux errors. Based on the digitized outputs of these controllers and the estimated spatial sector of the stator flux linkage vector, an optimal voltage vector is selected from a pre-defined switching look-up table [26]. This table maps the required corrective actions (increase/decrease) for both (torque/flux) and the flux position to one of the six active or two zero voltage vectors available from a standard two-level voltage source inverter. This direct selection mechanism results in fast torque dynamics and structural simplicity. However, a significant drawback of C-DTC is its variable switching frequency operation, which inherently leads to considerable torque and flux ripples and a broad harmonic spectrum, potentially causing acoustic noise and vibration issues [27].

It was demonstrated that rapid torque response is achieved by quickly changing the position of the stator flux linkage space vector with respect to the rotor flux space vector as (6) shows.

$$u_s = R_s i_s + \frac{d\psi_s}{dt} \Rightarrow \quad (6)$$

where, σ = 1 - Lm²/LsLr is leakage factor, Lm, Lr, Ls are mutual, rotor and stator inductances, Ψs, Ψr are stator and rotor flux, δ is the angle between rotor and stator flux vectors.

Rotor flux varies slowly because its rate of change relies on a larger rotor time constant; so, it is supposed to be fixed in a short period of time. The stator flux magnitude is also kept fixed. Rapid variation of torque can be gained if the stator flux space vector is varied quickly by quickly changing "δ". This is the concept of DTC. The instantaneous change of "δ" gained by switching on the appropriate stator voltage space vector of the VSI.

In the stationary reference frame, the stator flux linkage space vector can be obtained from the integration of the stator EMF. If the stator resistance voltage drop is neglected for simplicity, then the stator flux is the integration of the applied voltage. Hence, in a small period of time, the increment of the stator flux depends on the applied voltage. Then, the desired trajectory of the stator flux can be obtained by selecting the appropriate inverter output voltage vector.

$$\mathbf{u_s} = R_s\,\mathbf{i_s} + \frac{d\psi_s}{dt} \quad \text{then,}$$

$$\frac{d\psi_s}{dt} = \mathbf{u_s} - R_s\,\mathbf{i_s} \quad \text{then,}$$

$$\psi_s = \int (\mathbf{u_s} - R_s\,\mathbf{i_s})dt \quad (7)$$

It is seen from Equation (7) that the stator flux linkage space vector ($\underline{\Psi_s}$) can be controlled by changing the stator voltage ($\underline{u_s}$). Where, ($\underline{u_s}$) is one of the VSI eight voltage vectors.

For simplification, we can neglect the resistive voltage drop ($R_s\,\underline{i_s}$) then:

$$\underline{\Psi_s} = \int \underline{u_s}\,dt \quad (8)$$

Also, we can assume that the voltage vector remains constant for a small period of time (Δt), then:

$$u_s = \Delta t + \psi_s\,|_{t=0} \quad (9)$$

Where, $\underline{\Psi_s}\big|_{t=0}$: is the initial value of the stator flux linkage.

For a switch-on time (Δt), the increment of the stator flux can be given by:

$$\Delta\psi_s = u_s \cdot \Delta t \quad (10)$$

Therefore, the stator flux linkage space vector moves by $\Delta\,\Psi_s$ in the direction of the applied stator voltage vector, Fig. 1.

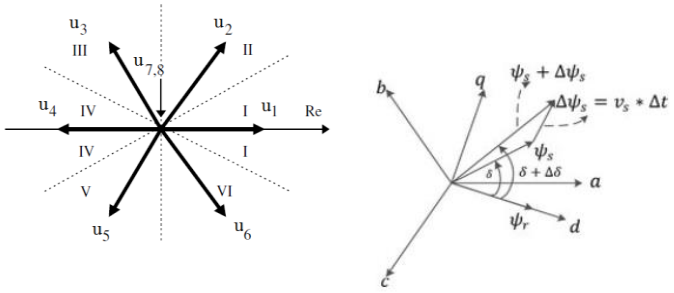

Fig. (1) Inverter Voltage Vectors and the Corresponding Flux Variation in Time Δt.

3.2 CONTROL OF STATOR FLUX-LINKAGE SPACE VECTOR MAGNITUDE

The suitable voltage vector needed to control the magnitude of the stator flux space vector is selected after dividing the plane into six sectors K(1) through K(6), Fig. 1., such that, [28]:

$$\frac{(2N-3)\pi}{6} \leq K(N) \leq \frac{(2N-1)\pi}{6} \qquad (11)$$

Where, N = 1, 2, 3 ……, 6. It is required to always keep the switching frequency as low as possible so that the most appropriate voltage vector is the one requires the minimum number of switching and drives both the stator flux and the torque errors in the required direction. In the k^{th} sector, the stator flux can be increased by applying one of the: k, k+1 (anticlockwise), or k-1 (clockwise) vectors. Therefore, flux can be increased by applying the voltage vector belongs to the sector or any of the adjacent voltage vectors. To decrease the stator flux, one of the voltage vectors is applied: k+2 (anticlockwise), k-2 (clockwise), or k+3. A deviation by a hysteresis band equal to $\pm\Delta\Psi_s$ is allowed for the actual flux with respect to the reference flux [28].

The block diagram of the conventional DTC of IM drive is shown in Fig. 2.

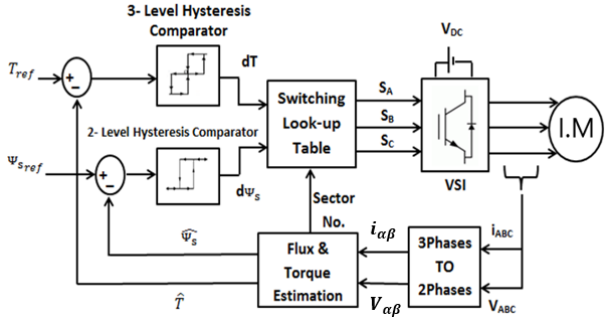

Fig. (2) Block Diagram of conventional DTC of IM drive

3.3. VOLTAGE SWITCHING LOOK-UP TABLE

It is a pre-designed table that receives its inputs from the torque and flux comparators in addition to the sector number to obtain the required voltage vector. There are different schemes of the switching table but the most common one is the one proposed by Takahashi et. al. It is given in Table .1. [29].

Suppose that the flux vector is in sector (1) and $d\Psi_s$ = 1& dT =1, then both of torque and flux are required to be increased. Therefore, u2 (110) is applied, Fig. 3. Note that u1 (100) can't be used as torque will be decreased as the torque angle seeks to be reduced. Now, $d\Psi_s$ = 1& dT =0, the flux doesn't be changed instantaneously and torque has the priority to be changed, then a zero voltage vector is applied that gives minimum switching states, u7 (111). Now, $d\Psi_s$ = 1& dT = -1, flux is needed to be increased and torque is needed to be reduced, then u6 (101) is applied. In the case of $d\Psi_s$ = 0 & dT =1, u3 (010) is applied to increase the torque. And so on [28].

Table .1. Voltage Switching Look-up Table

$d\Psi_s$	d_T	K(1)	K(2)	K(3)	K(4)	K(5)	K(6)
1	1	u_2	u_3	u_4	u_5	u_6	u_1
	0	u_7	u_0	u_7	u_0	u_7	u_0
	-1	u_6	u_1	u_2	u_3	u_4	u_5
0	1	u_3	u_4	u_5	u_6	u_1	u_2
	0	u_0	u_7	u_0	u_7	u_0	u_7
	-1	u_5	u_6	u_1	u_2	u_3	u_4

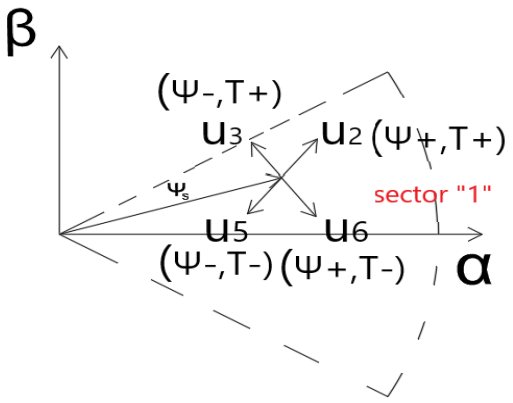

Fig. (3) Voltage Vector Selection Criteria

4. CONCEPT OF THE SPACE VECTOR MODULATION BASED DIRECT TORQUE CONTROL OF IMs

Space Vector Modulation-based Direct Torque Control (SVM-DTC) represents an advanced control strategy designed to improve the performance of induction motor drives by addressing the shortcomings of conventional Direct Torque Control (DTC). While traditional DTC methods are favored for their rapid dynamic response and straightforward implementation, they are often hindered by issues like high torque and flux ripples, fluctuating switching frequencies, and unwanted acoustic noise. SVM-DTC enhances the DTC framework by incorporating Space Vector Pulse Width Modulation (SVPWM) techniques, which replace traditional hysteresis controllers and lookup tables with a modulator that precisely determines the appropriate voltage vectors. This results in a steady switching frequency and a marked reduction in torque ripple, leading to smoother motor operation and higher system efficiency. Recent studies, highlight that integrating SVM with DTC not only improves control accuracy but also boosts energy efficiency in electric motor systems.

At its core, the concept of SVM-DTC revolves around the independent control of torque and stator flux through the use of voltage space vectors. In this method, the actual torque and flux values are continuously compared with the desired reference values. Instead of using hysteresis bands to trigger predefined voltage vectors, SVM-DTC employs a modulator that calculates the optimal voltage vector to apply during each sampling cycle.

This process enhances the precision of torque and flux control, guarantees a constant switching frequency, and reduces electromagnetic disturbances. Integrating intelligent control strategies within the SVM-DTC framework improves its adaptability to changes in load and motor parameters, making it especially effective in modern electric vehicle and industrial automation systems. These improvements make SVM-DTC a preferred approach for high-performance motor drives that demand precision, efficiency, and reliability [30]–[35]

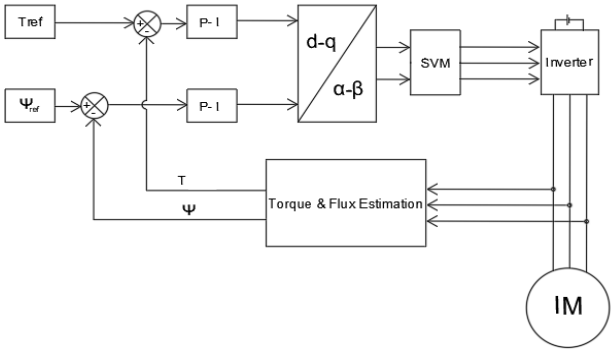

Fig(4) "SVM-DTC Block Diagram"

The block diagram of the SVM-DTC of IM is given in Fig(4). The principal aim of the Space Vector Modulation (SVM) strategy is the precise manipulation of inverter output voltage vectors to synthesize Pulse Width Modulated (PWM) waveforms possessing optimal harmonic characteristics. As illustrated in Figure 4, the reference command voltages for a three-phase inverter aggregate into a rotating space vector, denoted V*, which maintains a sinusoidal trajectory. This reference vector V* can be decomposed into components using the subsequent relationships:

$$V^{*}\sin\left(\frac{\pi}{3}-\alpha\right)=V_a\sin\left(\frac{\pi}{3}\right)$$

$$V^{*}\sin\alpha=V_b\sin\left(\frac{\pi}{3}\right) \qquad (12)$$

$$V_a=\frac{2}{\sqrt{3}}V\cdot\sin\left(\frac{\pi}{3}-\alpha\right)$$

$$V_b=\frac{2}{\sqrt{3}}V\cdot\sin(\alpha) \qquad (13)$$

Here, Va and Vb signify the constituent parts of the reference vector V* aligned along the axes of the adjacent active space vectors V1 and V2, respectively. A fundamental concept in SVM is that the average voltage generated by the inverter over a specific sampling interval, Tss, must equate to the command vector V*. This principle can be mathematically represented as:

$$\vec{V}^{*}=\vec{V}_a+\vec{V}_b=\vec{V}_1\cdot\frac{T_1}{T_{ss}}+\vec{V}_2\cdot\frac{T_2}{T_{ss}}+\vec{V}_0\cdot\frac{T_0}{T_{ss}}$$

Multiplying both sides by the sampling period T_{ss}, we get:

$$\vec{V}^{*}\cdot T_{ss}=\vec{V}_1\cdot T_1+\vec{V}_2\cdot T_2+\vec{V}_0\cdot T_0 \qquad (14)$$

The time intervals during which the adjacent active vectors (V1, V2) and zero vectors (V0/V7) are applied within the sampling period Tss are determined by the following calculations:

$$T_1=T_{ss}\cdot\frac{\sin\left(\frac{\pi}{3}-\alpha\right)}{\sin\left(\frac{\pi}{3}\right)},\quad T_2=T_{ss}\cdot\frac{\sin(\alpha)}{\sin\left(\frac{\pi}{3}\right)} \qquad (15)$$

Within this framework, the angle α relates the reference vector V* to the adjacent active vectors V1 and V2 (α = V*/V1 = V*/V2), while Tss designates the sampling duration. The terms T1, T2, and T0 specify the respective application times for the active vectors V1, V2, and the zero voltage vectors (V0 or V7) within one sampling interval Tss. Both V0 and V7 represent the null or zero states of the inverter. Furthermore, the magnitude of the active vectors relates to the DC link voltage as V1 = V2 = (2/3)VDC.

Based on these relationships, executing the standard Space Vector Pulse Width Modulation (SVPWM) algorithm traditionally requires several distinct steps. These include determining the correct operational sector, computing the necessary durations (T1, T2, T0) for the voltage vectors, translating these durations into precise switching instants for each inverter leg, and finally, generating the appropriate gate drive signals according to these leg timings. Consequently, the multitude of calculations and the sequential nature of the required algorithmic procedures contribute to the complexity and computationally demanding nature of the SVM implementation.

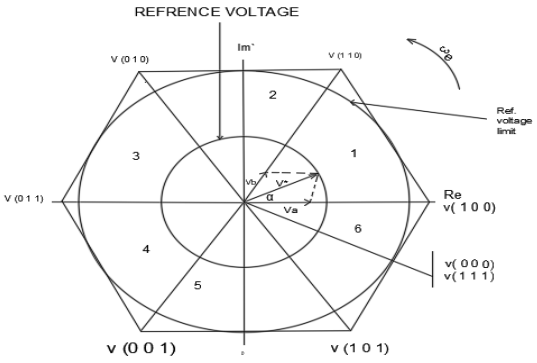

Fig. 5. Voltage space vector of 3 phase inverter.

5. RESULTS and DISCUSSIONS

In this section, comparisons between the conventional hysteresis DTC and SVM-DTC are made with the help of MATLAB/SIMULINK simulations to interpret the key differences between the two algorithms and outline their advantages and disadvantages when used in advanced electric drive systems. The used motor is a 200-HP power rating, 400V, 50 Hz with full parameter data and controller data outlined in Table 2 [36]. The Simulink models for the conventional DTC as well as the SVM-DTC schemas are shown in Fig (6), and (7) respectively.

Table.2 "Induction Motor Parameters"

Category	Parameter / Item	Value	Unit
Induction Motor (IM)	Rated Power	200	HP
	Rated Voltage	400	V
	Rated Frequency	50	Hz
	Stator Resistance (Rs)	14.85e-3	Ω
	Stator Inductance (Ls)	0.3027e-3	H
	Mutual Inductance (Lm)	10.46e-3	H
	Rotor Resistance (Rr)	9.295e-3	Ω
	Rotor Inductance (Lr)	0.3027e-3	H
	Inertia (J)	3.1	kg.m²
	Friction Coefficient (B)	0.08	N.m.s
Inverter	Type	IGBT / Diodes	-
Simulation/Base Control	Base Sample Time	2e-06	s (2 µs)
Speed Controller	Type	PI	-
	Proportional Gain (P gain)	30	-
	Integral Gain (I gain)	200	-
	Sampling Time	7 * 20e-6 = 140e-6	s (140 µs)
Hysteresis Controller	Torque Bandwidth (Hysteresis Band)	± 0.5	N.m
	Flux Bandwidth (Hysteresis Band)	± 0.01	Wb
	Maximum Average Switching Frequency	20	kHz
	Controller Sampling Time	2e-06	s (2 µs)

Upon initiating the simulation, several key waveforms can be monitored, including the stator current drawn by the motor, the resulting rotor speed and electromagnetic torque, and the voltage level of the DC bus. The commanded speed and torque values are also displayed for reference.

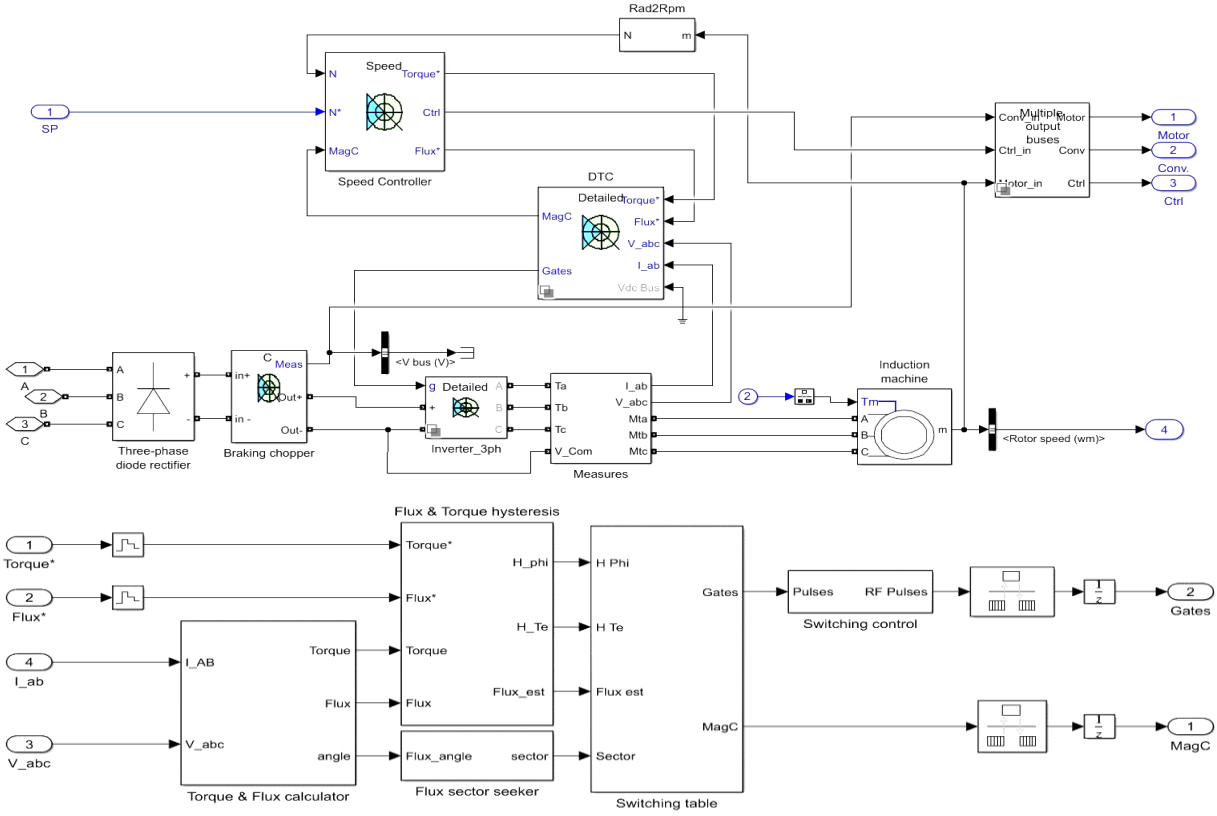

Fig(6) "Simulink Model of Conventional Hysteresis DTC of IM Drive"

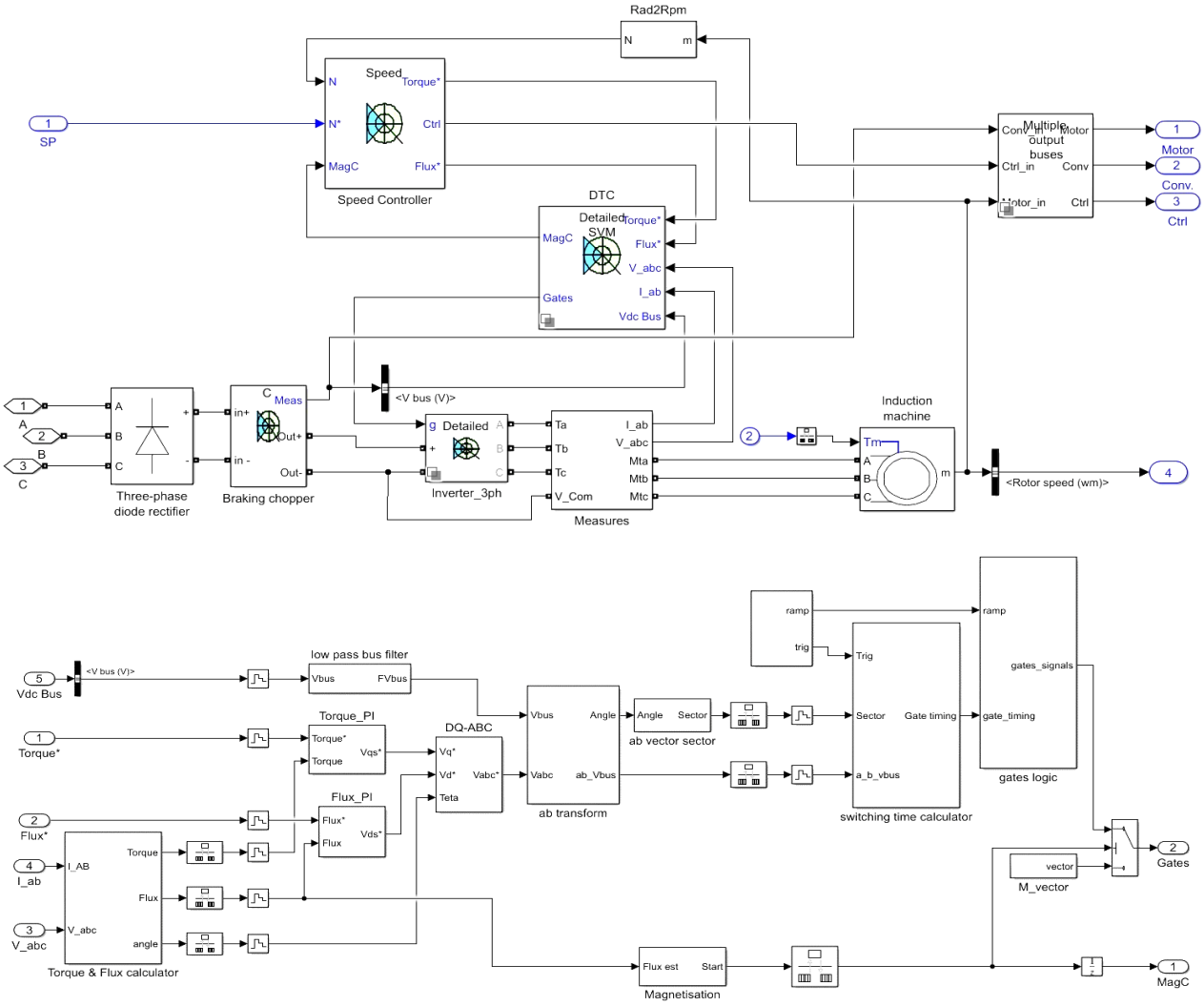

Fig(7) "Simulink Model of SVM-DTC of IM Drive"

The simulation sequence unfolds as follows:

- Initially (t=0s), a speed command of 500 rpm is issued. The drive accurately tracks the prescribed acceleration profile.
- Subsequently, at t=0.5s, the application of full rated load torque (equivalent to 792 N.m at nominal speed, though the text mentions 820 N.m as the final torque at 500 rpm) occurs while the motor accelerates. This disturbance causes the motor's electromagnetic torque to surge momentarily to its defined peak (1200 N.m) before settling at the required 820 N.m as the shaft reaches the target 500 rpm.
- At t=1s, the speed reference is changed to 0 rpm. The drive follows the deceleration profile with high fidelity.
- While decelerating, at t=1.5s, the mechanical load torque is abruptly reversed to -792 N.m. Despite this significant disturbance, the speed continues its controlled descent towards zero.
- Following the deceleration ramp, the motor's speed effectively stabilizes at 0 rpm.

Throughout these dynamic changes in speed and load, the effectiveness of the DC bus voltage regulation can be observed.

5.1 Results of the Conventional Hysteresis DTC:

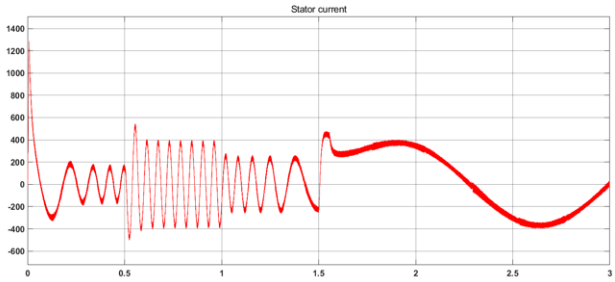

Fig(8) Stator Current of Conventional Hysteresis DTC

As shown from Fig(8), The current amplitude clearly reflects the motor's operating state. It's high during acceleration (0-0.75s) and deceleration (1s-2s) when high torque is demanded. It increases significantly at t=0.5s when the load is applied and decreases when the motor reaches steady speed (0.75s-1s) or near-zero speed (t>2s).

The sinusoidal envelope is visible, and its frequency correctly decreases as the motor speed reduces during deceleration (1s-2s).

Noticeable ripple is superimposed on the fundamental current waveform throughout the operation. This is partly due to the PWM inverter switching but is exacerbated by the nature of DTC's direct voltage vector application based on hysteresis bands.

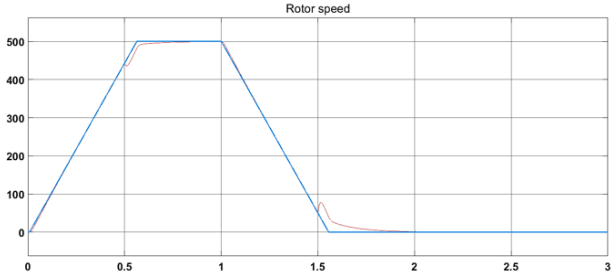

Fig (9) Rotor Speed of the conventional Hysteresis DTC

As shown from Fig(9), the actual rotor speed (red line) follows the reference speed ramp (blue line) with remarkable accuracy during both acceleration (0-0.75s) and deceleration (1s-2s).

The application of full load torque at t=0.5s and the abrupt load torque inversion at t=1.5s cause negligible deviation from the reference speed trajectory. This indicates excellent dynamic stiffness and load disturbance rejection capabilities of the combined speed control loop and the fast inner torque control provided by DTC.

The speed holds steady at 500 rpm between approx. 0.75s and 1s, and effectively settles at 0 rpm after t=2s.

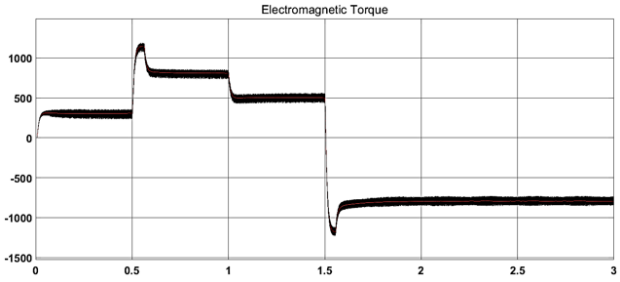

Fig (10) Torque of the conventional Hysteresis DTC

As displayed from Fig(10), the torque response is extremely fast. During acceleration (0-0.75s), it rapidly hits and maintains the maximum positive torque limit (approx. 1200 N.m). During deceleration (1s-2s), it quickly reverses and reaches the maximum negative (braking) torque limit (approx. -1200 N.m).

At t=0.5s, the torque stays at the limit as the motor still needs to accelerate and overcome the load. When the speed stabilizes (0.75s-1s), the torque drops precisely to the required steady-state load torque (approx. 820 N.m). It adapts quickly to the load inversion at t=1.5s while maintaining maximum braking effort.

This is the most defining characteristic of conventional DTC shown here. The actual torque exhibits substantial ripple around its average value throughout all operating phases (acceleration, steady-state, and deceleration). This ripple is a direct consequence of the hysteresis controllers constantly switching between voltage vectors to keep torque within the defined band (±0.5 N.m in this case, though the visual ripple looks larger). While the average torque control is excellent, these rapid fluctuations are inherent.

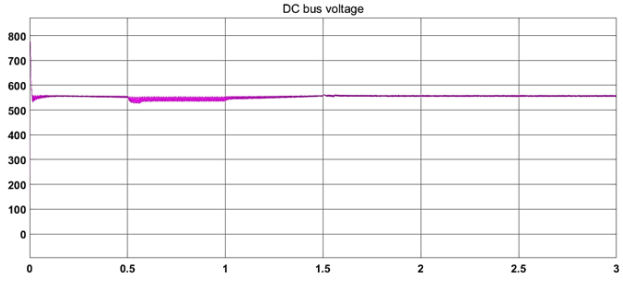

Fig (11) DC Bus Voltage for Conventional Hysteresis DTC

As shown from Fig(11) the DC bus voltage remains very well regulated around its nominal value (approx. 560-580V) throughout the entire simulation.

During deceleration (1s onwards), when the motor acts as a generator, the voltage shows only minor fluctuations. This indicates the braking chopper is effectively activating to dissipate the regenerated energy and prevent the DC bus voltage from rising excessively.

In Summary for Conventional DTC, These waveforms clearly illustrate the key features of conventional hysteresis-based DTC:

Extremely fast torque dynamics and excellent speed tracking/disturbance rejection capability.

However, significant torque ripple (and associated flux ripple, though not shown) is inherently present due to the hysteresis control mechanism. This also leads to ripple in the stator currents. The variable switching frequency associated with hysteresis control also contributes to challenges in filtering and potential acoustic noise.

5.2 RESULTS OF THE SVM- DTC SCHEME:

Let's analyze the following waveforms, assuming they represent the **SVM-DTC** scheme operating under the same conditions as the previously discussed Conventional DTC scenario.

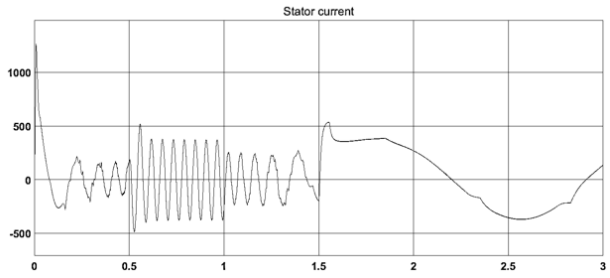

Fig(12) Stator Current in SVM-DTC Scheme

As seen in Fig(12), similar to the conventional DTC, the current amplitude correctly responds to the demands of acceleration, load application, steady-state operation, and deceleration. The AC nature and frequency variation with speed are evident.

A key visual difference is the apparent smoothness of the current waveform compared to the conventional DTC case. The high-frequency ripple superimposed on the fundamental component seems significantly reduced, resulting in a waveform closer to a pure sinusoidal, especially during steady-state periods (e.g., 0.75s - 1s).

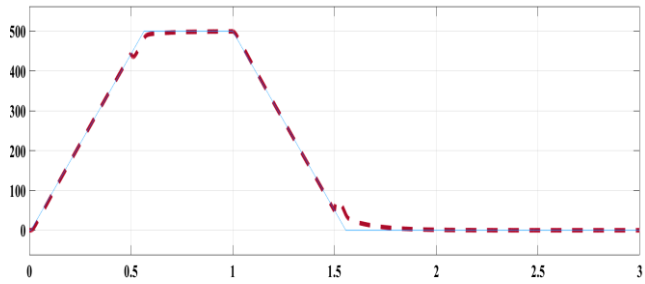

Fig(13) Rotor Speed in SVM-DTC Scheme

As shown in Fig(13), the actual speed (red) demonstrates precise tracking of the reference speed ramp (blue) during both acceleration and deceleration phases.

Load disturbances at t=0.5s (application) and t=1.5s (reversal) have minimal impact on the speed trajectory, indicating robust performance of the control loop.

The speed control performance appears virtually identical to the conventional DTC case in terms of tracking accuracy and disturbance rejection.

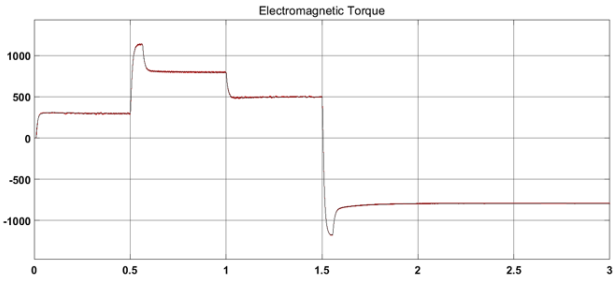

Fig (14) Electromagnetic Torque in SVM-DTC Scheme

As depicted from Fig(14), the torque response remains very rapid, quickly reaching the positive limit during acceleration and the negative limit during braking, and adapting swiftly to load changes at 0.5s and 1.5s.

This is the most striking improvement. Compared to the conventional DTC waveform, the torque ripple (the rapid fluctuation around the average or reference value) is dramatically reduced. The actual torque stays much closer to the commanded/average value (indicated by the blue reference line during transients and the settled value during steady state). This demonstrates the effectiveness of SVM in smoothing the torque output.

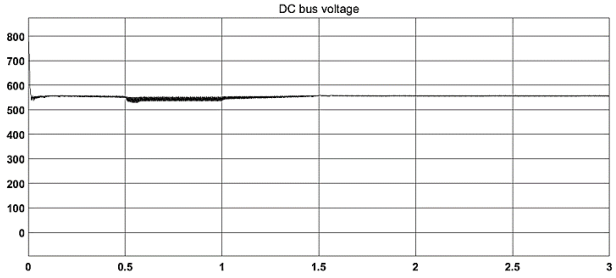

Fig (15) DC Bus Voltage in SVM-DTC Scheme

As displayed in Fig(15) , The DC bus voltage is maintained consistently around its nominal value throughout the simulation, similar to the conventional DTC case.

The voltage shows only minor, well-controlled fluctuations during the deceleration/regeneration phase (t > 1s), confirming proper operation of the braking chopper system.

5.3 COMPARISON: SVM-DTC VS. CONVENTIONAL (HYSTERESIS) DTC RESULTS

Based on the analysis of both sets of waveforms:

1. **Torque and Flux Ripple:** This is the most significant difference. SVM-DTC exhibits substantially lower torque ripple compared to conventional DTC. This translates to smoother motor operation, reduced mechanical stress, lower acoustic noise, and likely lower flux ripple as well (leading to more sinusoidal currents). The conventional DTC's torque waveform showed much larger, high-frequency fluctuations. SVM-DTC provides a 30% reduction in torque ripples and a 20% increased improvement in overall system efficiency compared to conventional hysteresis DTC.
2. **Current Quality:** The stator current waveform is visibly smoother and more sinusoidal in the SVM-DTC case, indicating a lower Total Harmonic Distortion (THD) compared to conventional DTC. This is a direct result of the reduced torque/flux ripple and the controlled voltage application via SVM.
3. **Switching Frequency:** Although not directly plotted, conventional DTC operates with a variable switching frequency dependent on operating conditions and hysteresis bands. SVM-DTC operates at a constant switching frequency determined by the SVM algorithm's sampling time. This predictability is advantageous for filter design and managing electromagnetic interference (EMI).
4. **Dynamic Response:** Both methods demonstrate excellent and very fast dynamic response in terms of speed tracking and torque control during transients (acceleration, deceleration, load changes). However, SVM-DTC achieves a 2% faster dynamic response time in reaching steady-state torque under transient conditions, highlighting its superior performance in real-time applications.
5. **Control Accuracy:** Both achieve accurate *average* speed and torque control. However, the steady-state precision of SVM-DTC is higher due to the drastically reduced ripple around the desired operating point.
6. **DC Bus Regulation:** Both schemes show effective DC bus voltage regulation when coupled with the braking chopper.
7. **Complexity:** While not visible in the waveforms, achieving the smoother performance of SVM-DTC requires a more complex algorithm involving PI controllers (typically for torque/flux error) and the SVM calculation itself, compared to the simpler hysteresis comparators and lookup table of conventional DTC.

6 CONCLUSIONS

The comparative results presented herein underscore the critical performance trade-offs associated with hysteresis-based and SVM-based Direct Torque Control strategies. While the simplicity and fast dynamics of the conventional method are appealing, its operational drawbacks, particularly ripple and variable switching frequency, limit its suitability for high-precision or noise-sensitive systems. The SVM-integrated approach demonstrably improves steady-state behavior and efficiency through controlled switching and reduced pulsations, despite its increased computational demands. These findings offer crucial guidance for optimizing drive system design in demanding sectors like industrial automation and automotive applications. Engineers can leverage this comparative assessment to select and potentially refine the DTC strategy that best aligns with specific objectives, whether prioritizing maximum dynamic capability or achieving enhanced control fidelity, efficiency, and system reliability.

SVM-DTC successfully addresses the main drawback of conventional DTC – the high torque and flux ripple – by employing Space Vector Modulation. This results in smoother torque delivery, more sinusoidal currents, and fixed-frequency operation, enhancing steady-state performance and potentially reducing noise and mechanical stress. Both methods provide excellent fast dynamic response, but SVM-DTC achieves this with significantly higher operational refinement, albeit with increased computational complexity.

8. REFERENCES

[1] Y. Yang, Q. Wang, and J. Shang, “Five-Level Hysteresis DTC of Open-End Winding Permanent Magnet Synchronous Motors with Zero-Sequence Currents Suppression and Torque Ripple Reduction,” IEEE Access, vol. 10, no. October, pp. 121762–121771, 2022, doi: 10.1109/ACCESS.2022.3223126.

[2] E. Benyoussef and S. Barkat, “Direct Torque Control Based on Space Vector Modulation With Balancing Strategy of Dual Star Induction Motor,” Rev. Roum. des Sci. Tech. Ser. Electrotech. Energ., vol. 67, no. 1, pp. 15–20, 2022.

[3] P. Singh and P. Gaur, “Grid interfaced solar water pumping system with improved space vector modulated direct torque control,” Ain Shams Eng. J., vol. 11, no. 4, pp. 1149–1162, 2020, doi: 10.1016/j.asej.2020.01.015.

[4] F. Ben Salem, M. T. Almousa, and N. Derbel, “Direct Torque Control with Space Vector Modulation (DTC-SVM) with Adaptive Fractional-Order Sliding Mode: A Path Towards Improved Electric Vehicle Propulsion,” World Electr. Veh. J., vol. 15, no. 12, pp. 1–15, 2024, doi: 10.3390/wevj15120563.

[5] T. G. Habetler, F. Profumo, M. Pastorelli, and L. M. Tolbert, “Direct Torque Control of Induction Machines Using Space Vector Modulation,” IEEE Trans. Ind. Appl., vol. 28, no. 5, pp. 1045–1053, 1992, doi: 10.1109/28.158828.

[6] C. Djamila, M. Yahia, C. Djamila, and M. Yahia, “Direct Torque Control Strategies of Induction Machine: Comparative Studies,” Direct Torque Control Strateg. Electr. Mach., Jan. 2020, doi: 10.5772/INTECHOPEN.90199.

[7] S. K. Gudey, M. Malla, K. Jasthi, and S. R. Gampa, “Direct Torque Control of an Induction Motor Using Fractional-Order Sliding Mode Control Technique for Quick Response and Reduced Torque

Ripple," World Electr. Veh. J. 2023, Vol. 14, Page 137, vol. 14, no. 6, p. 137, May 2023, doi: 10.3390/WEVJ14060137.

[8] N. El Ouanjli et al., "Improved twelve sectors DTC strategy of induction motor drive using Backstepping speed controller and P-MRAS stator resistance identification-design and validation," Alexandria Eng. J., vol. 80, pp. 358–371, Oct. 2023, doi: 10.1016/J.AEJ.2023.08.077.

[9] A. A. Kadum, "New adaptive hysteresis band width control for direct torque control of induction machine drives," Int. J. Power Electron. Drive Syst., vol. 11, no. 4, pp. 1908–1917, Dec. 2020, doi: 10.11591/IJPEDS.V11.I4.PP1908-1917.

[10] U. Mahanta, B. C. Mohanta, A. K. Panda, and B. P. Panigrahi, "Fuzzy logic-based direct torque control for improvement of the fault-tolerant drive of a five-phase induction motor," Trans. Inst. Meas. Control, vol. 43, no. 14, pp. 3120–3128, Oct. 2021, doi: 10.1177/01423312211015556;REQUESTEDJOURNAL:JOURNAL:TIMA.

[11] S. K. Gudey, M. Malla, K. Jasthi, and S. R. Gampa, "Direct Torque Control of an Induction Motor Using Fractional-Order Sliding Mode Control Technique for Quick Response and Reduced Torque Ripple," World Electr. Veh. J. 2023, Vol. 14, Page 137, vol. 14, no. 6, p. 137, May 2023, doi: 10.3390/WEVJ14060137.

[12] R. Rajendran and N. Devarajan, "A comparative performance analysis of torque control schemes for induction motor drives," Int. J. Power Electron. Drive Syst., vol. 2, no. 2, pp. 177–191, Jun. 2012, doi: 10.11591/IJPEDS.V2I2.207.

[13] N. Fazli and J. Siahbalaee, "Direct torque control of a wind energy conversion system with permanent magnet synchronous generator and matrix converter," 8th Power Electron. Drive Syst. Technol. Conf. PEDSTC 2017, pp. 166–171, Apr. 2017, doi: 10.1109/PEDSTC.2017.7910315.

[14] C. Murali and C. Chengaiah, "Direct Torque Control for Five-Phase Squirrel Cage Induction Generator in wind energy conversion systems based on Slip Angle," Proc. 6th Int. Conf. Commun. Electron. Syst. ICCES 2021, pp. 107–110, Jul. 2021, doi: 10.1109/ICCES51350.2021.9489128.

[15] J. Faiz, S. H. Hossieni, M. Ghaneei, A. Keyhani, and A. Proca, "Direct torque control of induction motors for electric propulsion systems," Electr. Power Syst. Res., vol. 51, no. 2, pp. 95–101, Aug. 1999, doi: 10.1016/S0378-7796(98)00098-4.

[16] Y. N. Tatte and M. V. Aware, "Direct Torque Control of Induction Motor with Common-Mode Voltage Elimination," Electr. Power Components Syst., vol. 44, no. 20, pp. 2310–2324, Dec. 2016, doi: 10.1080/15325008.2016.1220998.

[17] S. Kadam and P. P. Rajeevan, "Virtual Voltage Space Vector Based Direct Torque Control Scheme with Common Mode Voltage Elimination for Induction Motor Drives," 1st IEEE Ind. Electron. Soc. Annu. On-Line Conf. ONCON 2022, 2022, doi: 10.1109/ONCON56984.2022.10127005.

[18] T. Wang, C. Liu, G. Lei, Y. Guo, and J. Zhu, "Model predictive direct torque control of permanent magnet synchronous motors with extended set of voltage space vectors," IET Electr. Power Appl., vol. 11, no. 8, pp. 1376–1382, Sep. 2017, doi: 10.1049/IET-EPA.2016.0870.

[19] A. Jidin, N. R. N. Idris, A. H. M. Yatim, T. Sutikno, and M. E. Elbuluk, "A hybrid DTC-DSC drive for high performance induction motor control," J. Power Electron., vol. 11, no. 5, pp. 704–712, 2011, doi: 10.6113/JPE.2011.11.5.704.

[20] G. Banda and S. G. Kolli, "An Intelligent Adaptive Neural Network Controller for a Direct Torque Controlled eCAR Propulsion System," World Electr. Veh. J. 2021, Vol. 12, Page 44, vol. 12, no. 1, p. 44, Mar. 2021, doi: 10.3390/WEVJ12010044.

[21] S. Gdaim, A. Mtibaa, and M. F. Mimouni, "Artificial neural network-based DTC of an induction machine with experimental implementation on FPGA," Eng. Appl. Artif. Intell., vol. 121, p. 105972, May 2023, doi: 10.1016/J.ENGAPPAI.2023.105972.

[22] H. R. Khoei and E. F. Shahraki, "Fuzzy Logic Based Direct Power Control of Induction Motor Drive," Bull. Electr. Eng. Informatics, vol. 5, no. 3, pp. 296–306, Sep. 2016, doi: 10.11591/EEI.V5I3.538.

[23] F. Korkmaz, İ. Topaloglu, and H. Mamur, "Fuzzy Logic Based Direct Torque Control of Induction Motor With Space Vector Modulation," Int. J. Soft Comput. Artif. Intell. Appl., vol. 2, no. 6, pp. 33–42, Dec. 2013, doi: 10.5121/IJSCAI.2013.2603.

[24] D. Telford, M. W. Dunnigan, and B. W. Williams, "Comparison of Vector Control and Direct Torque Control of an induction machine," PESC Rec. - IEEE Annu. Power Electron. Spec. Conf., vol. 1, pp. 421–426, 2000, doi: 10.1109/PESC.2000.878893.

[25] M. A. W. Begh and H.-G. Herzog, "Comparison of Field Oriented Control and Direct Torque Control," Apr. 2024, doi: 10.36227/TECHRXIV.171332371.13141782/V1.

[26] G. S. Buja and M. P. Kazmierkowski, "Direct torque control of PWM inverter-fed AC motors - A survey," IEEE Trans. Ind. Electron., vol. 51, no. 4, pp. 744–757, Aug. 2004, doi: 10.1109/TIE.2004.831717.

[27] K. Chikh, M. Khafallah, A. Saad, D. Yousfi, and H. Chaikhy, "A novel fixed-switching-frequency DTC for PMSM drive with low torque and flux ripple based on sinusoidal pulse with modulation and predictive controller," Proc. 2012 Int. Conf. Multimed. Comput. Syst. ICMCS 2012, pp. 1069–1075, 2012, doi: 10.1109/ICMCS.2012.6320189.

[28] H. Abu-Rub, A. Iqbal, and J. Guzinski, "High performance control of AC drives with MATLAB/Simulink Haitham Abu-Rub, Atif Iqbal, Jaroslaw Guzinski," 2021.

[29] I. Takahashi and T. Noguchi, "A New Quick-Response and High-Efficiency Control Strategy of an Induction Motor," IEEE Trans. Ind. Appl., vol. IA-22, no. 5, pp. 820–827, 1986, doi: 10.1109/TIA.1986.4504799.

[30] M. M. Amin, F. F. M. El-Sousy, O. A. Mohammed, G. A. A. Aziz, and K. Gaber, "MRAS-Based Super-Twisting Sliding-Mode Estimator Combined with Block Control and DTC of Six-Phase Induction Motor for Ship Propulsion Application," IEEE Trans. Ind. Appl., vol. 57, no. 6, pp. 6646–6658, 2021, doi: 10.1109/TIA.2021.3115088.

[31] M. H. Holakooie, M. Ojaghi, and A. Taheri, "Direct Torque Control of Six-Phase Induction Motor with a Novel MRAS-Based Stator Resistance Estimator," IEEE Trans. Ind. Electron., vol. 65, no. 10, pp. 7685–7696, Oct. 2018, doi: 10.1109/TIE.2018.2807410.

[32] A. K. Peter, J. Mathew, and K. Gopakumar, "A Simplified DTC-SVPWM Scheme for Induction Motor Drives Using a Single PI Controller," IEEE Trans. Power Electron., vol. 38, no. 1, pp. 750–761, Jan. 2023, doi: 10.1109/TPEL.2022.3197362.

[33] U. R. Muduli, B. Chikondra, and R. K. Behera, "Space Vector PWM Based DTC Scheme with Reduced Common Mode Voltage for Five-Phase Induction Motor Drive," IEEE Trans. Power Electron., vol. 37, no. 1, pp. 114–124, Jan. 2022, doi: 10.1109/TPEL.2021.3092259.

[34] P. Kant and B. Singh, "A Sensorless DTC Scheme for 60-Pulse AC-DC Converter Fed 5-Level Six-Leg NPC Inverter Based Medium Voltage Induction Motor Drive," IEEE Trans. Energy Convers., vol. 35, no. 4, pp. 1916–1925, Dec. 2020, doi: 10.1109/TEC.2020.2997240.

[35] D.V. Makwana, "LSTM-ANN Intelligent Control Based onSpace Vector Modulated DTC for InductionMotor Drive," Int. J. Intell. Syst. Appl. Eng., vol. 12, no. 4, pp. 2254–2259, Jun. 2024, Accessed: Apr. 25, 2025. [Online]. Available: https://www.ijisae.org/index.php/IJISAE/article/view/6602

[36] H. Maghfiroh, J. S. Saputro, F. Adriyanto, A. Sujono, and R. L. Lambang, "Performance Evaluation of Fuzzy-PID in Speed Control of Three Phase Induction Motor," IOP Conf. Ser. Mater. Sci. Eng., vol. 1096, no. 1, p. 012071, Mar. 2021, doi: 10.1088/1757-899X/1096/1/012071.